Molecular Crystals and Liquid Crystals
Publication details, including instructions for authors and subscription information:
http://www.tandfonline.com/loi/gmcl16

Anisotropic Translational Diffusion of Methane and Chloroform in Thermotropic Nematic and Smectic Liquid Crystals

Michael E. Moseley [a] & Aharon Loewenstein [b a]
[a] Department of Isotope Research, The Weizmann Institute of Science, 76100, Rehovot, Israel
[b] Department of Chemistry, Technion-Israel Institute of Technology, Haifa, 32000, Israel
Version of record first published: 20 Apr 2011.

To cite this article: Michael E. Moseley & Aharon Loewenstein (1982): Anisotropic Translational Diffusion of Methane and Chloroform in Thermotropic Nematic and Smectic Liquid Crystals, Molecular Crystals and Liquid Crystals, 90:1-2, 117-144

To link to this article: http://dx.doi.org/10.1080/00268948208076176

Mol. Cryst. Liq. Cryst., 1982, Vol. 90, pp. 117–144
0026-8941/82/9002-0117$06.50/0

Printed in the United States of America

Anisotropic Translational Diffusion of Methane and Chloroform in Thermotropic Nematic and Smectic Liquid Crystals

MICHAEL E. MOSELEY†

Department of Isotope Research, The Weizmann Institute of Science, 76100 Rehovot, Israel

and

AHARON LOEWENSTEIN

Department of Chemistry, Technion-Israel Institute of Technology, Haifa, 32000, Israel

(*Received May 6, 1982; in final form July 14, 1982*)

Nuclear magnetic resonance pulsed-gradient spin-echo measurements are reported for the anisotropic translational diffusion coefficients and their temperature dependence, of methane, monodeuteromethane and chloroform dissolved in several thermotropic liquid crystals exhibiting nematic, smectic A and smectic B phases. For methane, in those liquid crystals forming only nematic phases, the diffusion parallel to the director ($D_{\parallel}$) is greater than the perpendicular diffusion ($D_{\perp}$); the magnitude of the diffusional anisotropy ($D_{\parallel}/D_{\perp}$) depends on the nature of the nematic medium. In the nematic phases of smectic-forming materials, $D_{\parallel}/D_{\perp} < 1$. In the smectic A phases, $D_{\parallel}/D_{\perp} \ll 1$ with a much larger activation energy for $D_{\parallel}$. In the smectic B phase, $D_{\parallel}/D_{\perp} \ll 1$ with similar activation energies. Chloroform exhibits similar behavior with deviations in the nematic phases of a polymorphic liquid crystal. A qualitative interpretation of these results is given in terms of several factors which govern the diffusion behavior: different diffusion characteristics in aliphatic and aromatic regions of the ordered medium, expulsion of methane (and possibly chloroform) from the aromatic cores into the aliphatic end chains as a result of the smectic layering behavior and pronounced pretransitional ordering effects in nematic phases of the polymorphic liquid crystals. In addition to the diffusion measurements, proton dipolar and deuterium quadrupolar splittings in these systems are reported for

† Sir Charles Clore Postdoctoral Fellow 1981–1982

CH_4 and CH_3D. These splittings are related to the strength of solute-solvent interaction and consequently to the diffusion patterns. Complementary data is presented for methane proton spin-lattice relaxation measurements in these systems.

INTRODUCTION

Nuclear magnetic resonance spin-echo measurements of translational diffusion coefficients of small solute molecules dissolved in ordered thermotropic liquid crystal mesophases have been scarce[1-7] and only several[4-6] have yielded reliable values of the diffusional anisotropy. The value of these measurements is due to the fact that the diffusion behavior of small molecules is a very sensitive probe to the liquid crystalline intermolecular potentials and thus provides additional information to that obtained by diffusion and other studies of the liquid crystal molecules themselves. Furthermore, relaxation studies on the molecular reorientation of small solutes in anisotropic environments of liquid crystal mesophases indicate[8] that the understanding of the low frequency spectral densities may require knowledge of the molecular diffusion rates.

Spin-echo diffusion measurements apply either a steady-state[9] or a pulsed magnetic field gradient[10] along one of the axes in the laboratory frame, using either anti-Helmholtz[9] or quadrupolar gradient coils.[11] The anisotropy of diffusion, $D_\parallel/D_\perp$, or the diffusion along the orientational director $D_\parallel$ *vs.* diffusion perpendicular to the director $D_\perp$, can be measured using Helmholtz coils by rotation of the sample tube in the magnetic field,[3] assuming that the mesophase does not reorient during the time of the measurement. This precludes studies in the nematic phase and in some smectic phases. The quadrupole coil itself may be rotated in order to apply the gradient in different directions relative to the magnetic field,[2,4-6] assuming that no misalignments or field homogeneity changes occur. To optimize the relative accuracy, the pulsed-gradient spin-echo diffusion measurements reported herein employed two separate but similar quadrupole coils mounted together in a fixed orientation in the magnetic field, to generate pulsed gradients along the z and x axes in the laboratory frame.

In all the studied systems, $\Delta\chi > 0$ and thus the liquid crystal molecular director of each mesophase aligns along (parallel to) the magnetic field (z magnet axis). The measured coefficients of diffusion in the direction of the magnetic field, D_z, are therefore denoted as $D_\parallel$, the diffu-

sion coefficient parallel to the director. Similarly, the diffusion perpendicular to the field in the x direction, D_x, describes translation perpendicular to the director and is denoted as $D_\perp$.

The diffusion coefficients of methane in the nematic and solid phases of *p*-methoxybenzylidene-*n*-butylaniline (MBBA) have been reported[7] to be on the order of 5×10^{-8} m^2s^{-1} and found to be relatively temperature and phase independent. As this behavior contrasts greatly to other solute diffusion measurements in liquid crystals[1-6] and to methane diffusion in isotropic solvents,[12-13] it was decided to reinvestigate the methane diffusion and its anisotropy in MBBA and compare this to the behavior in the nematic and smectic phases of other liquid crystals. Methane is a much smaller probe molecule than any other previously studied in a mesophase and does little to disturb the environment, as evidenced by the fact that no appreciable phase transition temperature depressions are observed in methane-liquid crystal solutions. However, proton and deuterium NMR spectra of methane and monodeuteromethane in oriented mesophases do show small dipolar and quadrupolar splittings, indicating solute-phase interactions.[14-16] Knowledge of how these interactions correlate with methane diffusion behavior in the different phases of a variety of liquid crystal systems should be of interest and assist to understand not only the nature of the interactions but also the degree of the directional motional constraints acting on probe molecules in ordered phases.

Complementary information on the dynamic behavior of small solutes in liquid crystals may be obtained from proton spin-lattice relaxation (T_1) measurements. There exist, however, major difficulties in their interpretation and correlation with diffusion data, for the reason that proton T_1 values are influenced by both translational and rotational motional processes, which involve both intra- and intermolecular interactions.[17] Nevertheless, a qualitative inspection of the relaxation behavior is instructive and is therefore included in this study.

In this paper we report then, the anisotropic diffusion behavior of methane and monodeuteromethane in the following nematic liquid crystals: *p*-methoxy-*n*-alkylazoxybenzene mixture (Merck Licrystal Phase 5), MBBA and *p*-*n*-heptylcyanobiphenyl (7CB). These measurements are compared to results from the nematic and smectic A (S_A) phases of *p*-*n*-octylcyanobiphenyl (8CB) and to the nematic, S_A and smectic B (S_B) phases of *p*-butylbenzylidene-*n*-hexylaniline (40.6). Further, methane and monodeuteromethane proton and deuterium lineshapes, and methane proton T_1 relaxation rates are discussed in relation to the diffusion results. Finally, in an effort to ascertain the ef-

fect of solute size and composition, diffusion measurements are reported on dilute chloroform solutions in the solvents Phase 5 and *p*-butoxybenzylidene-*n*-octylaniline (40.8). Chloroform is larger than methane, having over twice the molecular volume, while retaining a roughly-spherical shape. It is more polar than methane and is known to form short-lived complexes with aromatic groups. Also, the relaxation behavior of chloroform in Phase 5 has been thoroughly studied.[8]

EXPERIMENTAL

Methane and monodeuteromethane were purchased from Merck. Chloroform was spectral grade from BDH. The liquid crystals MBBA (Eastman), Phase 5 (Merck), 7CB and 8CB (BDH) were used without further purification. The liquid crystals 40.6 and 40.8 were prepared in the manner described in references 18–19 from *p*-*n*-butoxybenzaldehyde and *p*-*n*-hexylaniline (40.6) and *p*-*n*-octylaniline (40.8). The phase transition temperatures of the liquid crystals were similar to literature values.

Samples were prepared in 5 mm o.d. (3.4 mm i.d.) pyrex NMR tubes. The liquid crystal (about 0.18 ml) was first degassed afterwhich methane or monodeuteromethane was introduced at pressures of approximately 9 or 15 atm. respectively. Chloroform was added to make 2.5 wt% (7.8 mole%) solutions. The tubes were sealed and left at room temperature for at least one week prior to measurement. Before each measurement series, the sample was heated into the isotropic phase, shaken vigorously in a vortex stirrer and allowed to cool very slowly in the magnetic field from the isotropic phase with temperature cycling at the transition temperatures. Each measurement in the series was then done at a progressively lower temperature allowing the sample at least 15 min. to establish thermal equilibrium. The concentrations of methane and monodeuteromethane dissolved in the samples have been determined from their signal intensities relative to the known chloroform concentrations in similar samples and are estimated to be 4 mole % CH_4 and 6 mole % CH_3D, which corresponds to about or less than 1 wt %. No appreciable changes in solute concentration were observed in either 8CB, 40.6 or 40.8 upon cooling from the nematic to smectic phases. The measured transition temperature differences between methane and monodeuteromethane samples were within 1°C. The methane solution phase transitions occurred over a 0.5–1.0°C interval and were typically within 1°C of solvent literature values. Hence, the effects of

pressure at the 9–15 atm levels in these studies are not seen to be important considerations to the liquid crystal solvent properties. Table I lists the liquid crystal solvent-solute systems studied as well as their observed phase transition temperatures.

All proton and deuterium lineshape experiments were performed on a Bruker WH-270 NMR spectrometer operating at 270 MHz and 41 MHz respectively. Relaxation and diffusion measurements were performed on the CH_4, CH_3D or $CHCl_3$ protons at 90 MHz on a Bruker WH-90 NMR spectrometer. The temperature was controlled

TABLE I

Solvent and solute structural formulae and corresponding observed solution phase transition temperatures. The letters *I*, *N*, S_A and S_B denote the isotropic, nematic, smectic A and smectic B phases respectively. Phase 5 is a mixture of 60% $n = 2$ (Phase 4) and 40% $n = 0$.

SOLVENT	SOLUTE	TRANSITIONS (°C)
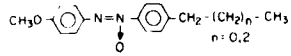 PHASE 5	CH_4	N → I 72.3
	$CHCl_3$	N → I 54.2
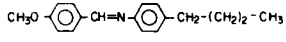 MBBA	CH_4	N → I 44.0
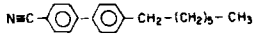 7CB	CH_4	N → I 40.5
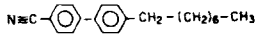 8CB	CH_4	S_A → N → I 33.0 40.0
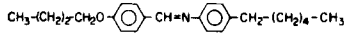 406	CH_4	S_B → S_A → N → I 46 55.2 75.5
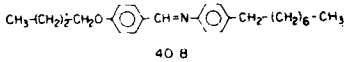 408	$CHCl_3$	S_B → S_A → N → I 39 55.0 74.0

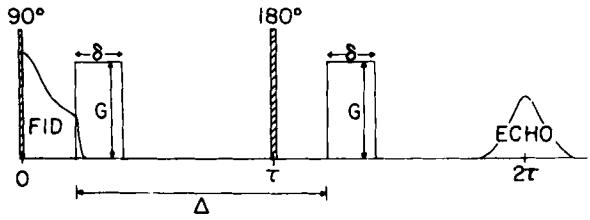

FIGURE 1 The pulse sequence for the determination of translational diffusion by the pulsed-gradient spin-echo technique. A magnetic field gradient pulse of strength G and duration δ is applied in the interval τ between the 90° and 180° rf pulses. After a time Δ from the onset of the first gradient pulse, a second identical pulse is applied. Echo signals are recorded as a function of δ only. Diffusion occurring during the time Δ will attenuate the echo according to Equation 1.

with a Bruker BST 100/700 unit, which was calibrated before each measurement series with a Fluke 2190 digital thermometer. The precision between temperature measurements was typically 0.1°C while the absolute accuracy is estimated at ±1°C. A laboratory-built deuterium external lock was used to stabilize the WH-90 magnetic field.

The nonselective inversion recovery 180°-τ-90° pulse sequence was used in T_1 measurements (pulse repetition time $> 5T_1$). For the diffusion measurements, the Stejskal-Tanner pulsed-gradient spin-echo pulse sequence[10] was used. The pulse sequence and timing parameter symbols are shown in Figure 1. To measure the diffusion parallel and perpendicular to the magnetic field, D_z and D_x respectively, the pulsed gradients were applied, in separate experiments, along the z and x magnet axes as shown in Figure 2. The gradients were generated by passing current pulses of 1.4 A through the appropriate coil in the twin-quadrupole coil assembly shown in Figure 2. The general scheme of quadrupole coil construction are given in Ref. 11 and 20–22. Each quadrupole coil consisted of 10 turns of 34 AWG coated magnet wire per quadrant. The two separate coils were wound at exactly 45° to one another and mounted together on a thin mylar sheet around the outside of the cylindrical glass insert dewar within the 5 mm Bruker proton fixed-frequency probe. The diameter of the coils was 23 mm and the length 55 mm. Great care was taken to ensure proper alignment of the coil assembly within the probe. The assembly was vertically positioned around the rf coil (diameter 7 mm and height 3 mm) afterwhich the orientation, as shown in Figure 2, was fixed and not moved throughout the measurements. Care was also taken to position sample tubes such that the sample height was evenly distributed within the rf-quadrupole coil geometry.

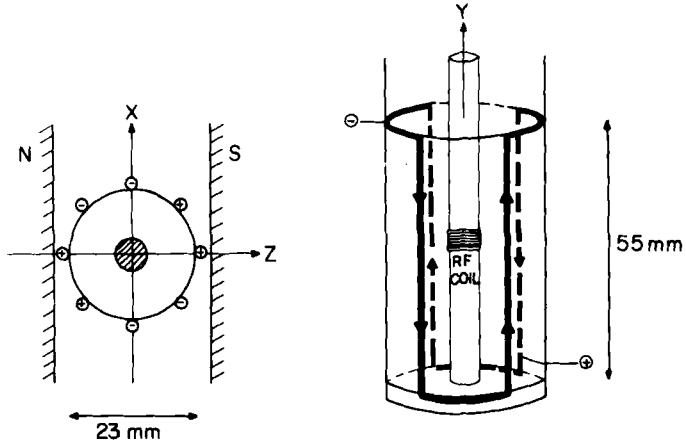

FIGURE 2 Practical design of the z and x quadrupole field gradient coils. On the left, in the transverse cross section, the x coil is shown with its four parallel wire bundles on the x and z axes with the alternating current directions denoted as + (current down) and − (current up). The z gradient coil, identical to the x coil, lies with bundles situated on the diagonals. On the right, the z coil is shown mounted on the dewar insert around the rf coil and sample tube guide. The arrows indicate current direction.

The resistance of each gradient coil was 3 ohms. The coils were pulsed by a simple, laboratory-built, software-controlled transistor switch circuit, shown in Figure 3. The switch circuit was controlled directly from the pulse program of the Nicolet 1180 minicomputer interfaced to the WH-90, powered by a precision stabilized 12 A power supply and matched via the current-limiting resistor R (Figure 3) to the quadrupole coil. The appropriate coil was manually connected to the

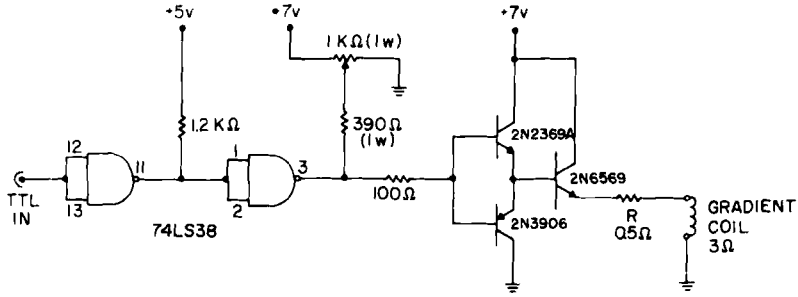

FIGURE 3 Schematic of the TTL—transistor current-switch circuit used to generate the z and x pulsed field gradients through the corresponding quadrupole coil. The 1kΩ potentiometer and current-limiting resistor R determine the current pulsed through the coils.

circuit before each D_z or D_x measurement. The rise and fall times for the coils were about 100 μs at the maximum 1.4 A level. During the maximum pulsed-gradients intervals used in these experiments (27.4 ms), no current pulse drop or other abnormality could be observed.

Prior to each experimental series, several long gradient pulses were applied to induce long-term residual gradients,[23] afterwhich the field homogeneity was maximized. This was a precautionary measure since residual gradient effects were never observed. Linewidths in the non-spinning 3.4 mm i.d. sample tubes were typically 2 Hz. Each diffusion experiment consisted of 12–14 measurements in which the pulsed gradient duration, δ, was varied from 1.4 ms to 27.4 ms. Values of Δ, the time interval between the gradient pulse leading edges, were typically 30.4 ms to 90.4 ms and were always chosen to allow for a delay of at least 15.4 ms between the completion of a gradient pulse and the 180° rf pulse or the echo data sampling. This was done to minimize any effects of short-term residual gradients.[23] For each measurement, 1 to 4 spin echoes were accumulated 200–500 Hz off-resonance with a quadrature phase detection scheme afterwhich the latter half of the echo was Fourier transformed with about 5 Hz exponential weighing. The FT signal intensities which corresponded to the spin-echo intensities (I_i) were then fitted to the equation

$$I_i = I_o \exp(-2\tau/T_2) \exp[-\gamma_H^2 G_i^2 D_i \delta^2(\Delta - \delta/3)] \qquad (1)$$

using a nonlinear least-squares analysis (error limits correspond to 95% confidence intervals, regarding random errors only), where γ_H is the proton magnetogyric ratio and the other parameters are explained in Figure 1. To eliminate the T_2 term in the above equation, the 90°–180° interval, τ, was held fixed such that $\tau = \Delta$. Typical error limits are represented by error bars in the figures.

The Δ and δ values from the pulse programmer were reproducible to within 2 μs. Unfortunately, the shortest allowable programmable delay was 1.4 ms, thus precluding an absolute gradient strength calibration.[23-24] The gradient calibrations were performed after each measurement series on a reference sample of spectral-grade cyclohexane at 25.0°C ($D = 1.475 \times 10^{-9}$ m^{2}s^{-1}),[25] under identical conditions to those used in the experimental series. The gradients have also been calibrated at various gradient pulse current settings and average coil constants were measured to be 6.3 ± 0.1 G/cm$A$ and 5.8 ± 0.1 G/cm$A$ for the x and z coils respectively. This corresponds to $G_x = 8.9 \pm 0.2$ G/cm and $G_z = 8.2 \pm 0.2$ G/cm for these experiments ($A = 1.4$ ampere). As a test of the orthogonality of the two applied z and x axis gradients, the

anisotropy of methane diffusion in the smectic B phase of 40.6 at 26.8°C is shown in Figure 4. The two left spectra show typical D_z ($D_\parallel$) and D_x ($D_\perp$) experiments. The sample tube was then rotated 90° which interchanges the z and x directions and the experiments were repeated. The measured values before and after rotation were identical within experimental error and found to be $D_x = 0.86\ (\pm 0.06) \times 10^{-9}\ m^2 s^{-1}$ and $D_z = 0.040\ (\pm 0.003) \times 10^{-9} m^2 s^{-1}$.

Local material inhomogeneities in the smectic phases might affect the measured diffusion values. To prevent this as much as possible the samples were thermally treated in the manner described above.

RESULTS AND DISCUSSION

A. Methane diffusion in Phase 5 and MBBA.

Measurements of the diffusion coefficients of methane in Phase 5 as functions of the inverse absolute temperature are shown in Figure 5. The Fourier transformed signals in the nematic phase show only the methane resonance as the Phase 5 resonances are too broad to be observed. Corresponding diffusion coefficients for CH_3D in Phase 5 were within the experimental error limits for methane diffusion, despite the pressure difference. The temperature dependent anisotropy of methane diffusion is easily observed and varied from $D_\parallel/D_\perp = D_z/D_x = 1.2$ at 68.7°C to 1.3 at 24.2°C. Plots of ln D against inverse absolute temperature were linear and the activation energies for methane diffusion are listed in Table II.

The diffusion of methane in MBBA is shown in Figure 6 as function of the inverse absolute temperature. Again, no difference in the diffusion behavior was observed for methane and monodeuteromethane. Above the clearing point both the methane and MBBA resonances were observed, which allowed determination of $D_\parallel$ and $D_\perp$ for both compounds. All MBBA resonances gave identical values of $D_\perp$ and $D_\parallel$ was found to be equal to $D_\perp$ within experimental error. The diffusion of the solvent MBBA is approximately an order of magnitude slower than that of methane, with absolute values similar to those that were obtained in the isotropic phase by Blinc *et al.*[26] and by Krüger and Spiesecke.[4] In the nematic phase, the anisotropy of methane diffusion varied from $D_\parallel/D_\perp = 1.1$ at 42.5°C to 1.2 at 18.2°C, slightly less than corresponding values in Phase 5. Arrhenius plots of methane diffusion against inverse temperature are linear and the activation energies are listed in Table II.

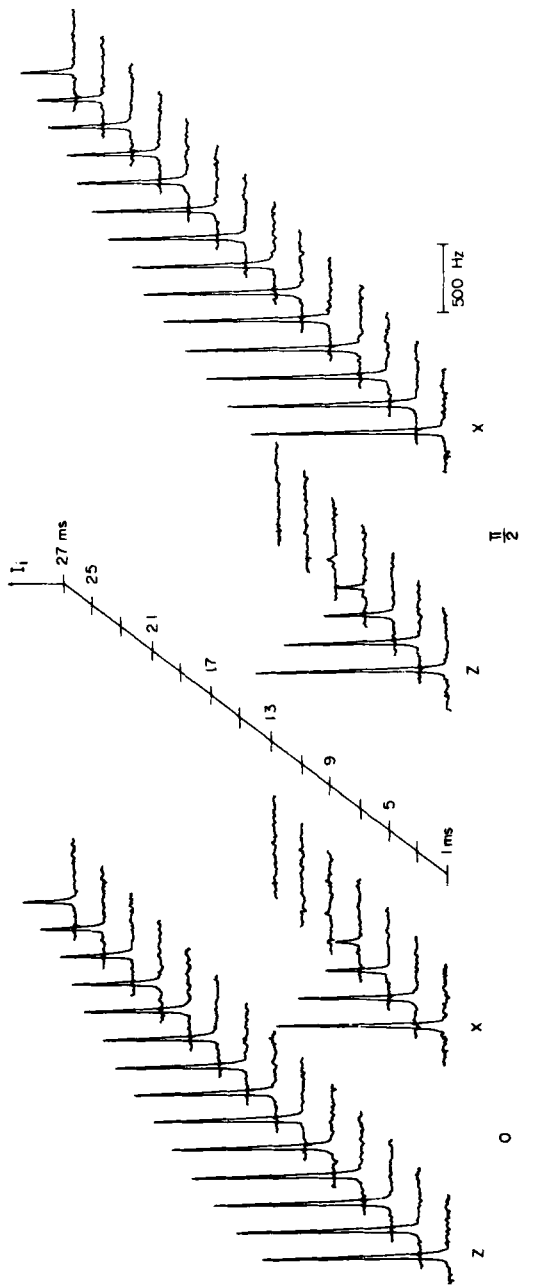

FIGURE 4 Typical diffusion experiments on methane in the smectic B phase of 40.6 at 26.8°C. The CH_4 proton FT signal intensities, I_i, are shown as functions of the pulsed field gradient duration, $\delta = 1.4$-27.4 ms, directions of diffusion (z and x magnet axes) and sample tube rotation in radians). $\Delta = 90.9$ ms, $G_x = 8.9$ gauss/cm and $G_z = 8.2$ gauss/cm. Four spin echoes were accumulated prior to Fourier transformation with 5 Hz artificial broadening.

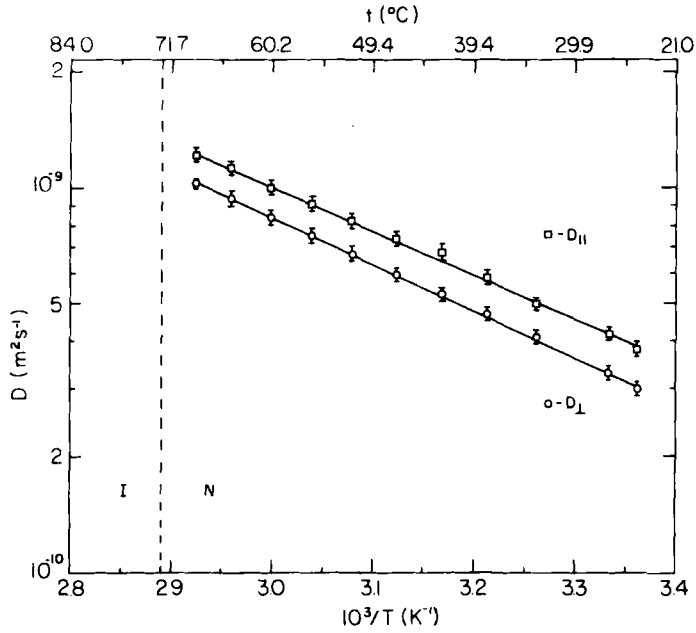

FIGURE 5 Arrhenius plots of methane diffusion coefficients in Phase 5. Methane diffusion parallel and perpendicular to the director are denoted as $D_{\parallel}$ (squares) and $D_{\perp}$ (circles) respectively. The isotropic (I)-nematic (N) phase transition temperature is indicated by the vertical broken line. The lines through the points are best fits used in determining the activation energies for diffusion.

In comparison to the results in Figures 5 and 6, methane diffusion in the normal alkanes (C_5-C_{10}) is typically 4–9 $\times$ 10^{-9} m^2s^{-1} at 25°C with activation energies of about 2–4 kcal/mole.[12-13] Methane diffusion in a nematic phase is thus considerably slower than in simple solvents and suggests that its translation is sensitive to the nature of the environment. Further, the values of methane diffusion in MBBA (Figure 6) deviate greatly from the much higher values reported previously.[7] It is now quite certain that both the diffusion and relaxation data reported previously[7] are erroneous and resulted from an error in the experimental procedure.

In the only other similar study involving anisotropic solute diffusion in nematic phases, Krüger and Spiesecke[4] measured the diffusion coefficients for CCl_2CF_2 (DDE), CCl_3CF_3 (TTE) and $(CH_3)_4Si$ (TMS) at 2 wt % concentrations in Phase 4 and also TMS in MBBA. Phase 4 and Phase 5 have very similar properties as solvents: Phase 5 (Table I) is a

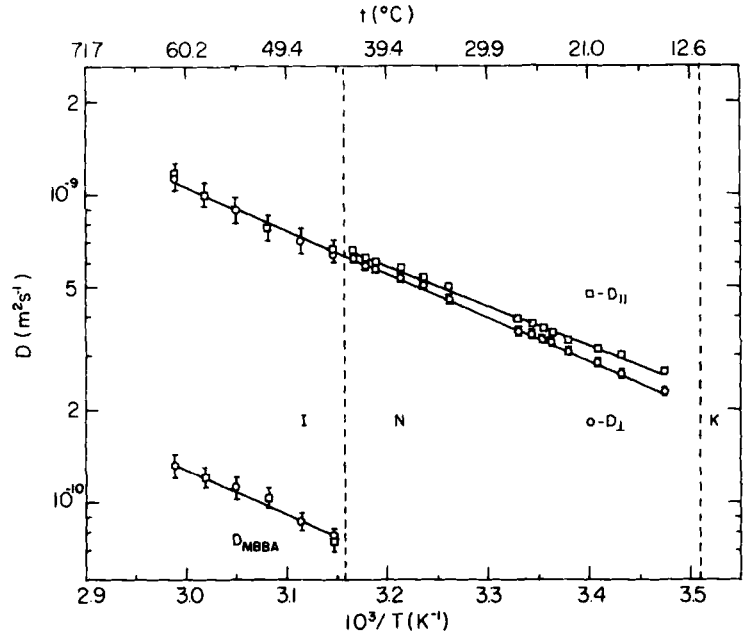

FIGURE 6 Arrhenius plots of methane diffusion (upper curves) in MBBA. Diffusion of MBBA in the isotropic phase is also shown. Transitions between the isotropic (*I*), nematic (*N*) and solid (*K*) phases are indicated by the vertical broken lines.

mixture of 60% *p*-methoxy-*n*-butylazoxybenzene (Phase 4) and 40% *p*-methoxy-*n*-ethylazoxybenzene. The respective clearing points (T_c) for Phase 4 and Phase 5 are 74°C and 73°C. Likewise, the specific gravities and capillary viscosities are similar: 1.12 g/cm^2 vs. 1.12 g/cm^2 and 30 cSt vs. 27.5 cSt at 20°C respectively.[27] Comparing our results with those of Krüger and Spiesecke several trends become clear: it is apparent that for dilute solutes in nematic phases, diffusion along the director is slightly faster than diffusion perpendicular to it. The roughly parallel, uniaxial arrangement of the solvent molecules, which are much bulkier and diffuse considerably slower, acts as an effective anisotropic barrier to solute translation in which the diffusing solute encounters fewer hindrances along the director than in the plane normal to it. Further, the rate of solute diffusion in Phase 4/5 and MBBA is inversely proportional and the corresponding activation energies (Table II) proportional, to the "size" (volume) of the solute. The correlation of diffusion rates with solute size has been widely studied in isotropic liq-

TABLE II

Activation energies of methane and chloroform diffusion in the isotropic (I), nematic (N), smectic A (S_A) and smectic B (S_B) phases of liquid crystal solvents.

Solvent	Phase	$E_\parallel$ (kcal/mole)	$E_\perp$ (kcal/mole)
		CH_4	
Phase 5	N	5.3 ± 0.2	5.5 ± 0.2
MBBA	I	6.8 ± 0.5	6.8 ± 0.5
	N	6.1 ± 0.2	6.5 ± 0.2
7CB	I	6.6 ± 0.7	6.6 ± 0.7
	N	see text	6.1 ± 0.3
8CB	I	6.6 ± 0.6	6.6 ± 0.6
	N	8.3	1.9
	S_A	11.9 ± 0.4	4.7 ± 0.4
40.6	N	7.6 ± 0.3	3.4 ± 0.2
	S_A	33 ± 2	see text
	S_B	3.0 ± 0.3	4.9 ± 0.2
		$CHCl_3$	
Phase 5	N	6.1 ± 0.3	6.6 ± 0.3
40.8	N	7.7 ± 0.4	6.3 ± 0.4
	S_A	16 ± 1	1.3 ± 0.2
	S_B	2.0 ± 0.5	5.2 ± 0.5

uids [28,29] though rarely with solutes smaller than the solvent molecules and no studies have appeared for anisotropic solvents. It is also noticed that $E_\perp > E_\parallel$ ($E_\perp/E_\parallel \sim 1.1$) for all solutes studied in the nematics. These trends are clearly functions of the anisotropic nature of the solvent, though other related factors such as the degree of solvent ordering, specific solvent-solvent and solute-solvent association, etc. are certainly involved. It seems reasonable to assume that the observed temperature dependence of the solute diffusional anisotropy is related to solvent ordering both of which increase with decreasing temperature. No known comparative study of the molecular ordering of Phase 5 and MBBA has been performed to our knowledge.

The translational diffusion coefficients $D_\parallel$ and $D_\perp$ of a dilute solute in a nematic phase can be related through a Stokes-Einstein type relation to the corresponding solvent Helfrich "translational"[32] viscosities parallel and perpendicular to the flow, η_2^H and η_3^H respectively. One advantage in relating diffusion to the viscosity of the medium is that unknown effects due to solvent ordering, solvent-solvent interactions and solvent mobility are already taken into account through their contribution to the viscosity coefficients. In recent papers by Kneppe *et al.*,[30,31] values of the anisotropic Helfrich viscosity coefficients have been re-

ported for MBBA and Phase 4 as functions of temperature. At any given temperature, the ratio of the perpendicular to parallel flow viscosities η_3^H/η_2^H can be defined as the anisotropy of viscosity and is greater in Phase 4 than in MBBA. In fact, in the temperature range over which Phase 4/5 and MBBA may be compared, the ratios of the viscosity anisotropies in Phase 4 to that in MBBA are roughly equal to the corresponding ratios of the solute diffusional anisotropies.

It is observed but not readily apparent why the activation energies for solute diffusion are greater in MBBA than in Phase 4/5 by a factor of about 1.1–1.2 for both TMS[4] and methane. Kneppe *et al.*[30,31] found a greater activation energy of viscosity in isotropic MBBA than in isotropic Phase 4. Although the η_2^H and η_3^H behavior for Phase 4 and MBBA were similar at temperatures below about 25°C, the relative changes in η_2^H and η_3^H over a comparible range were greater for MBBA than for Phase 4, due to the large variation of the order parameter in MBBA near the clearing point.

B. Methane diffusion in 7CB and 8CB

The measurements of methane diffusion in 7CB and 8CB are shown in Figure 7. In the isotropic phase, the diffusion of the 7CB solvent molecules was slightly faster than that of 8CB, and both solvents were found to diffuse at comparable rates to MBBA (Figure 6). Methane diffusion behavior in the isotropic phases of 7CB and 8CB were similar and comparable to the corresponding behavior in MBBA. In 7CB, which lacks a smectic phase the methane diffusion behavior in the nematic phase is similar to that in Phase 5 and MBBA where $D_\parallel > D_\perp$, although the anisotropy is much smaller, reaching a maximum of about 1.05 just below the clearing point. The average methane diffusional anisotropies in Phase 5, MBBA and 7CB were found to be 1.25, 1.15 and 1.05 respectively. This suggests that a correspondence may exist to the nematicity or to the nematic ranges of these solvents, which are 78°, 25° and 14 °C respectively.

The dominant feature of the methane diffusion behavior in 7CB is the clear "switch-over" at 27°C below which $D_\parallel$ becomes progressively smaller than $D_\perp$. It will be shown later than in smectic-forming nematics, $D_\perp > D_\parallel$ for methane and therefore this behavior may be related to a reported short-range layering in 7CB which is described[33] as a quasi-smectic A ordering on a local scale due to strong molecular association and pronounced head-to-tail alignment. This alignment forms[34] bulky dipolar centers of cyanobiphenyl cores which, when aligned in layers

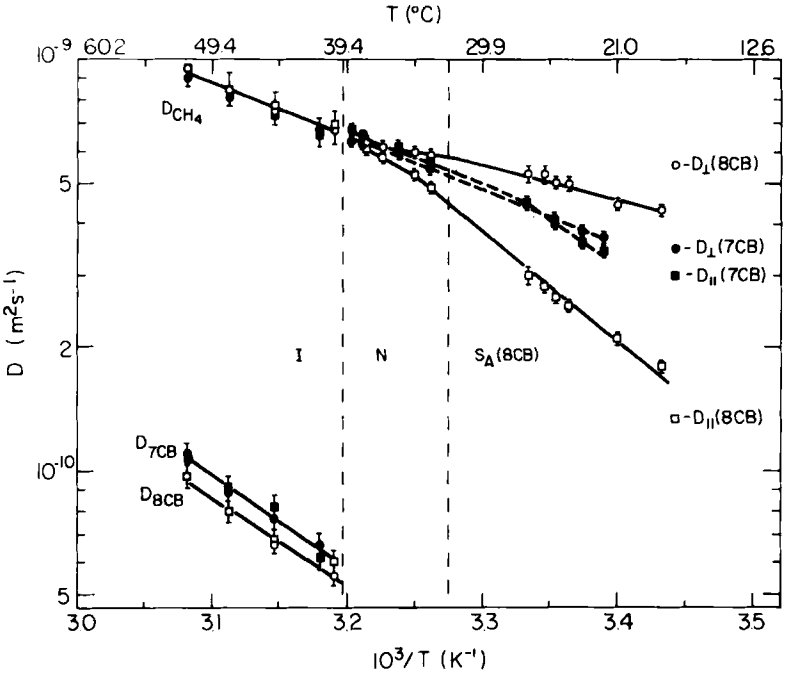

FIGURE 7 Arrhenius plots of methane diffusion in 7CB and 8CB. Diffusion of 7CB and 8CB in the isotropic phase is also shown (bottom). $D_\perp$ (circles) and $D_\parallel$ (squares) denote methane diffusion perpendicular/parallel to the director in 7CB and 8CB. The isotropic (I)-nematic (N) transition temperatures were similar for both 7CN and 8CB. The dashed and solid lines through the points in the nematic and smectic A phases are best fits used in the determination of the activation energies in 7CB and 8CB respectively.

normal to the director would tend to impede methane diffusion along the director while not drastically affecting transverse diffusion. The temperature dependence of $D_\perp$ is linear in an Arrhenius plot with a calculated activation energy $E_\perp = 6.1 \pm 0.3$ kcal/mole, whereas that of $D_\parallel$ becomes nonlinear below 27°C.

Methane diffusion in polymorphic 8CB (Figure 7) differs drastically from 7CB. This is certainly due to the existence of a smectic A phase below the short nematic interval. The longitudinal diffusion, $D_\parallel$, only approaches $D_\perp$ in the nematic phase. Further, $E_\perp = 1.9$ kcal/mole is much smaller than that expected for solute diffusion in nematic phases (Table II). Other studies have shown [32] that in the case of a weakly first order $N \rightarrow S_A$ phase transition, strong pretransitional effects from smectic ordering can be present well into the nematic phase. Here the pretransitional effects are twofold: the smectic bilayer formation of the

cyanobiphenyls hinders diffusion parallel to the director (diffusion from layer to layer) while allowing rapid transverse diffusion within the layer. Both effects contribute to the observation that $D_\perp > D_\parallel$ and $E_\parallel > E_\perp$ throughout the nematic phase. The extent to which longitudinal flow is affected by the $N \rightarrow S_A$ pretransitional effects can also be observed in the η_2^H *vs.* η_3^H behavior in the nematic phase of 8CB.[31] While the transverse viscosity, η_3^H shows normal behavior down to the phase transition, η_2^H is very sensitive to the pretransitional smectic order and begins to rise asymptotically at temperatures well into the nematic phase.

Below the phase transition, the sharp decrease in $D_\parallel$ is due to the increasing formation of the smectic bilayering at progressively lower temperatures and is reasonably well accounted for by the greater affinity of methane toward the aliphatic tail regions than toward the strongly dipolar aromatic cores. Steric effects from the packing should also be considered. Despite the very small size of methane compared to the 8CB solvent molecules, the strong head-to-tail association and alignment of the aromatic cores would greatly limit methane translation in this region. Methane diffusion in the S_A phase is probably one of slow longitudinal penetration of the central cores with faster liquid-like motion within the layers. The activation energy for transverse methane diffusion in 8CB is $E_\perp = 4.7$ kcal/mole, similar to that observed in the lighter alkanes. The longitudinal activation energy is listed in Table II as $E_\parallel = 11.9$ kcal/mole.

C. Methane diffusion in 40.6

Results for the diffusion of methane in 40.6 are given in Figure 8. The behavior is similar but much more pronounced than that found in 8CB and suggests that pretransitional smectic layering has a profound effect on the longitudinal methane diffusion in the nematic phase. The smooth decrease in $D_\parallel$ through the transition suggests that the formation of the central core packing is relatively continuous. This is supported by the smooth temperature dependence of the liquid crystal molecular ordering through the transition found in the similar homologue, 40.8.[35]

The observed value $E_\parallel = 33$ kcal/mole in the S_A phase of 40.6 indicates a much tighter packing with decreasing temperature than that observed for 8CB. The large activation energies for transverse solute diffusion in the S_A phase (Table II) are similar to those found in studies by Krüger and co-workers[5,6] involving CCl_3CF_3 (TTE) in *p*-hexanoyl

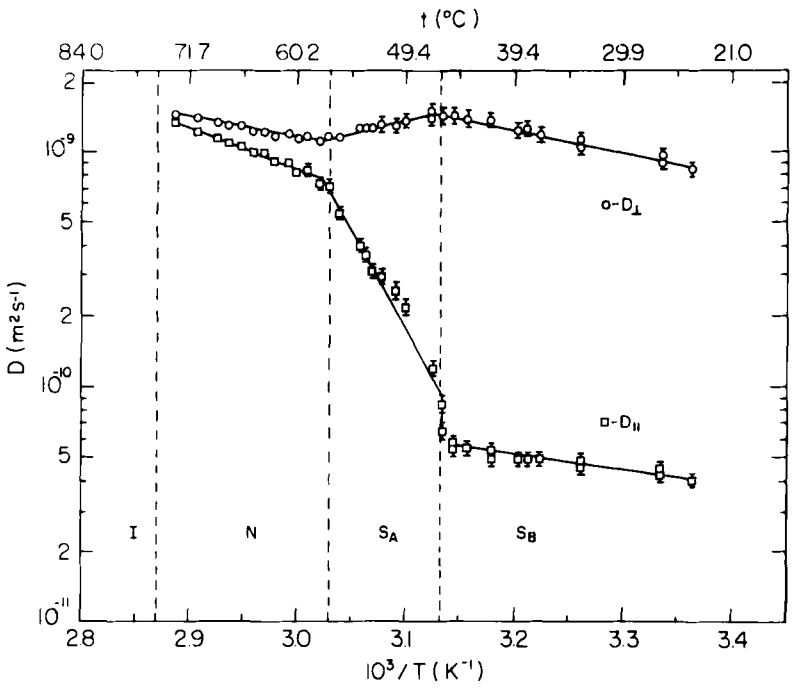

FIGURE 8 Arrhenius plots of methane diffusion in the isotropic (*I*), nematic (*N*), smectic A (S_A) and smectic B (S_B) phases of 40.6.

and *p*-dodecanoylbenzylidene-*p'*-aminoazobenzene, where solute longitudinal diffusion in the S_A phase required activation energies on the order of 20–30 kcal/mole. These studies and the results from Figure 8 sharply contrast and question an early study by Murphy *et al.*[3] who found essentially no change in $D_\parallel$ for TMS (5–10 mole %) in 40.8 throughout the S_A and S_B phases.

Chu *et al.*[36] have proposed a quantitative model to calculate the ratio $D_\perp/D_\parallel$ of spherical impurities in smectic A phases. They calculate the effective masses, $m_\perp$ and $m_\parallel$ of an impurity particle interacting with acoustic phonons which are present along a preferred direction. The effective masses are simply related to the diffusion constants through the Einstein relation. We have tried unsuccessfully to apply these calculations to our results of CH_4 diffusion in 40.6; the reasons being the difficulty in estimating the parameter C_1/a, the interaction energy and its temperature dependence. Furthermore, it is believed that the fair agreement which Chu *et al.* obtained with the results of Murphy *et al.* is probably fortuitous.

The abrupt decrease in $D_{\parallel}$ for methane in 40.6 at the $S_A \rightarrow S_B$ transition is probably a result of the strongly first-order formation of close-packed, crystalline-like layering observed in X-ray studies of the S_B lamellar solids.[37,38] The low $D_{\parallel}$ values and activation energy ($E_{\parallel} = 4.5$ kcal/mole) in the S_B phase indicates a pseudo-solid lattice jump process across the layer barriers. This result is similar to that found for TTE in the S_B phase of *p*-dodecanoylbenzylidene-*p'*-aminoazobenzene.[6]

The activation energy for transverse methane diffusion in the nematic phase of 40.6 ($E_{\perp} = 3.4$ kcal/mole) is lower than expected, compared to the corresponding values in the nematic phases of Phase 5, MBBA and 7CB. It is, however, similar to that in 8CB and reflects the large influence that local smectic ordering exerts on the methane diffusion behavior in nematic phases of polymorphic liquid crystals.

Transverse methane diffusion in the S_A phase of 40.6 was found to *increase* with decreasing temperature throughout the phase. Similar experiments on monodeuteromethane in 40.6 showed an identical behavior. The influence of increasing smectic order in the S_A phase would tend to decrease the activation energy for transverse diffusion, as was reasoned above for 8CB, although this is most likely not the sole factor involved. Rather, a methane expulsion process, resulting from layer packing, coupled with smectic layering might explain these results. Methane seems to be gradually expelled from the densely-packed aromatic regions to the non-polar regions within the layer. Lin and Freed[39] use such an expulsion argument to explain the anomalous ordering and relaxation behavior found for the spin-probe PD-Tempone in the S_A phases of 40.6 and 40.8. They did not, however, observe such an effect in 8CB and reasoned this to be due to the opposing trends in the S_A phase is thus a weighted average described by the true diffusion NO.M liquid crystals. This may also explain why no increase in methane diffusion was observed in the 8CB S_A phase. The bilayer structure in 8CB is described[39] as being characterized by a layer structure that expands with decreasing temperature, whereas this spacing in 40.6 contracts. In 40.6, a layer contraction would promote methane expulsion. This plus the shift in methane concentration to the aliphatic region, due to the greater affinity of methane toward nonpolar sites, leads to the observed increase in $D_{\perp}$ with decreasing temperature. In 8CB however, the slight increase in spacing may decrease the expulsion effect to the extent that only a decreased activation energy for transverse methane diffusion is observed.

In the S_A phases of 8CB and 40.6, the observed temperature dependence of the diffusion coefficients most likely does not follow a simple Arrhenius behavior. This is so because the diffusion process is coupled

to the expulsion process which may have a different temperature dependence. The observed diffusion coefficient at a given temperature in the S_A phase is thus a weighted average described by the true diffusion temperature dependence plus a term involving the equilibrium between sites. It is therefore obvious that the "activation energy" described herein for solute diffusion in S_A phases should be referred to as an "apparent" activation energy.

With the onset of the $S_A \rightarrow S_B$ phase transition, the 40.6 sample is frozen into a solid-like crystalline phase. The expulsion process is most likely complete and the transverse diffusion exhibits a simple Arrhenius behavior with $E_\perp = 4.7$ kcal/mole, which is characteristic of methane diffusion in an aliphatic environment similar to that of dodecane.[12,13]

D. Dipolar and quadrupolar splittings in CH_4 and CH_3D

Proton or deuterium spectra of CH_4 or CD_3D dissolved in nematic phases are known to exhibit dipolar or quadrupolar splittings.[14-16] Proton spectra of CH_4 show a 1:3:3:1 quartet and a 1:2:1 triplet for CH_3D while deuterium spectra show a 1:1 doublet. The proton splittings of CH_3D are considerably larger than those of CH_4 which may re-

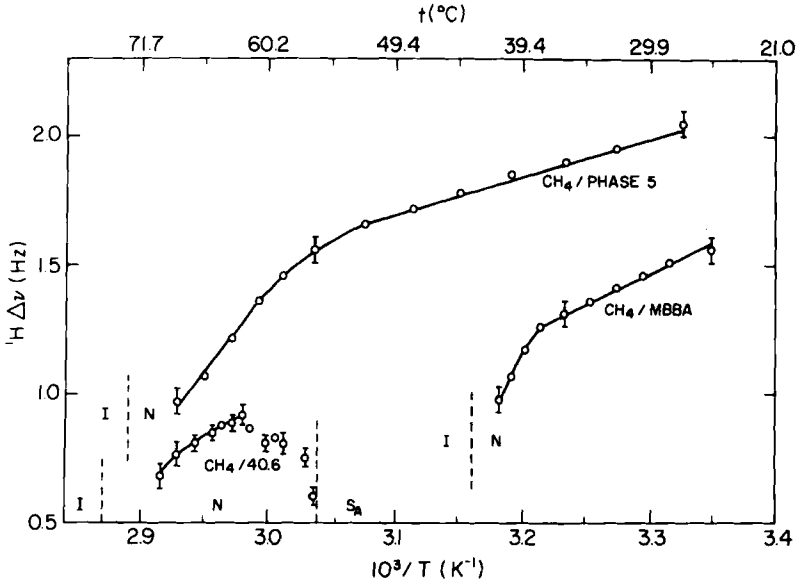

FIGURE 9 Temperature dependence of the proton splitting, $^1H\Delta\nu$, of CH_4 in Phase 5, MBBA and 40.6. The splitting is defined as the distance in Hz between the central doublet in the observed 1:3:3:1 quartet. Vertical broken lines indicate observed isotropic (I), nematic (N) and smectic A (S_A) phase transitions.

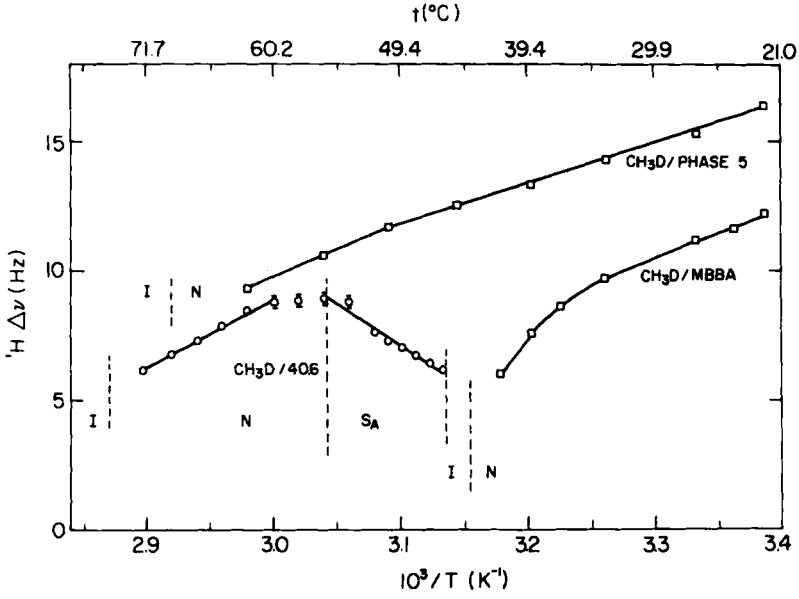

FIGURE 10 Temperature dependence of the proton splitting, $^1H\Delta\nu$, of CH_3D in Phase 5, MBBA and 40.6. The splitting was measured as the distance in Hz between the center and downfield signals in the 1:2:1 triplet. The use of broken and solid lines is explained in Figure 9.

flect the slight deviation from tetrahedral symmetry when one proton is substituted by a deuteron. Figures 9, 10 and 11 show the temperature dependences of the CH_4 proton, CH_3D proton and CH_3D deuterium splittings in the systems under study. Proton spectra of the CH_4 dissolved in 7CB and 8CB are an exception as the observed signals were not split; presumably the splittings were too small to be observed.

Attempts to interpret these splittings in terms of molecular order parameters are rather complex[40] because of the high symmetry of the solutes. Still, it is believed that the magnitude of the splittings is related to the strength of the anisotropic solute-solvent interactions and consequently a correlation might be sought to the observed anisotropy of the diffusion coefficients. Comparison between the diffusion data shown in Figures 5–7 and the corresponding splittings in Figures 9–11 does indeed suggest that a correlation exists. The relative magnitudes of diffusion anisotropies and the dipolar or quadrupolar splittings in the nematic phases of Phase 5, MBBA and 7CB show proportionality. Assuming that larger splittings would be observed for methane located in a more ordered region the proportionality may be related to the nematicity of the solvent.

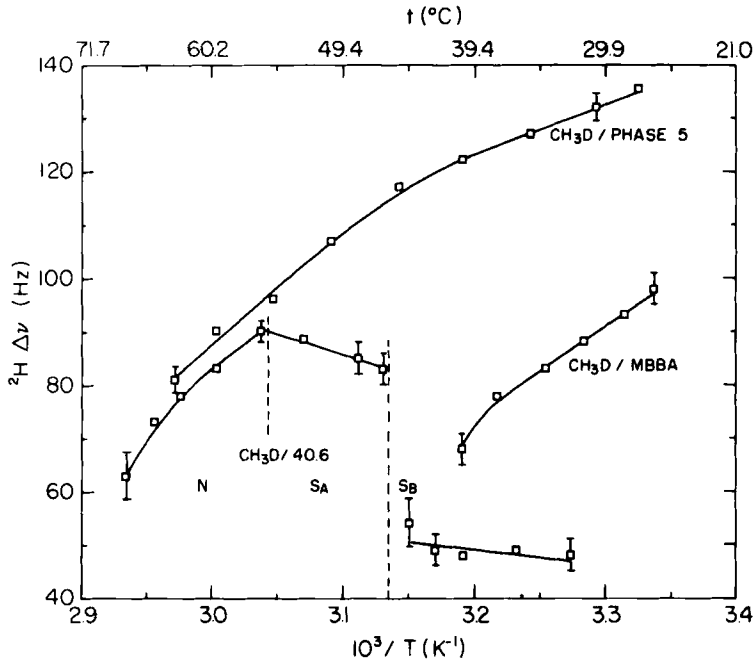

FIGURE 11 Temperature dependence of the deuterium splitting $^2H\Delta\nu$, in CH_3 in Phase 5, MBBA and 40.6, where the splitting is the frequency difference in Hz between the signals in the 1:1 doublet. The vertical broken lines indicate the nematic (N), smectic A (S_A) and smectic B (S_B) phase transitions in 40.6.

The behavior of the splittings (which is more pronounced in the quadrupolar spectra) in the nematic and smectic phases of 40.6 show a striking similarity to the diffusion data in Figure 8. The $N \rightarrow S_A$ pretransition effect and the S_A methane expulsion effect are clearly evident in Figures 9–11. The CH_4 proton lineshapes in Figure 12 show the linewidth behavior upon cooling from the nematic phase. In the S_A phase the splitting collapses with no apparent increase in the linewidth, supporting the picture of methane expulsion to the aliphatic regions with enhanced mobility. The large increase in the linewidth as the sample is cooled from 53°C (S_A) to 47°C (S_B) reflects the drastic decrease in flexibility experienced by the aliphatic tails as the material is frozen into the crystalline S_B phase.

E. Proton spin-lattice relaxation of CH_4

Proton spin-lattice relaxation rates of CH_4 and CH_3D in MBBA and Phase 5 are shown in Figure 13 and those of CH_4 in 40.6 in Figure 14. Measurements in MBBA and Phase 5 (Figure 13) give fairly linear Ar-

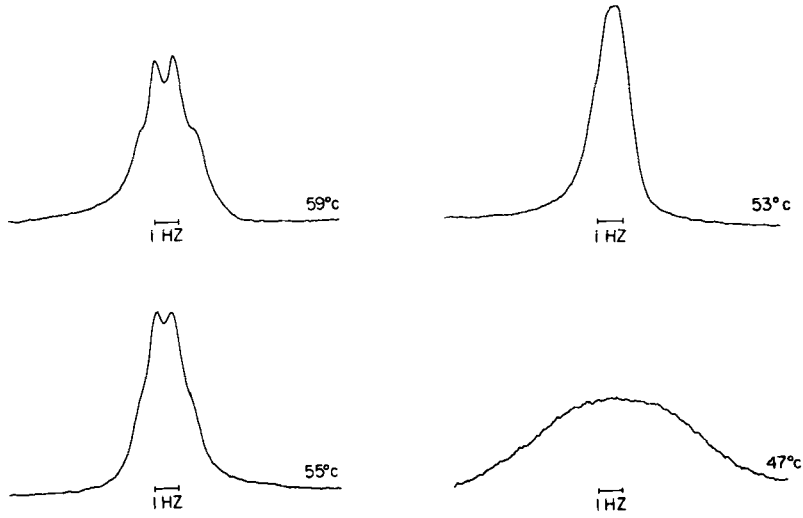

FIGURE 12 Proton lineshapes of CH_4 as a function of temperature in the nematic (55°C), smectic A (53°C) and smectic B (47°C) phases of 40.6.

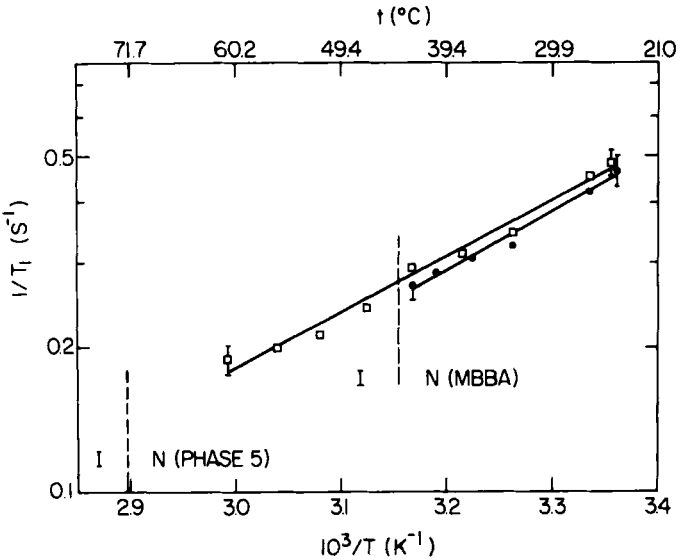

FIGURE 13 Proton spin-lattice relaxation rates ($1/T_1$) for CH_4 in Phase 5 (squares) and MBBA (circles) as functions of the inverse absolute temperature.

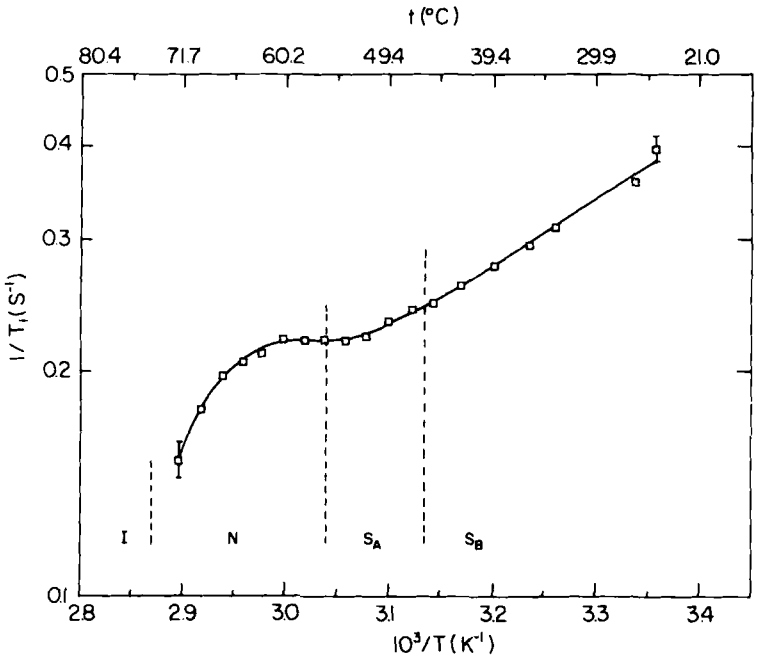

FIGURE 14 Proton spin-lattice relaxation rates ($1/T_1$) for CH_4 in 40.6 as a function of inverse absolute temperature.

rhenius plots with activation energies slightly smaller than the corresponding values for either $D_{\parallel}$ or $D_{\perp}$. Assuming that T_1 processes are largely determined by rotational processes, these results indicate a lower barrier to rotational than to translational processes.

The behavior of the proton T_1 values of CH_4 in 40.6 is quite different and has some unusual features: the Arrhenius plot in the nematic phase is not linear, starting with a rather large activation energy (*ca* 8 kcal/mole) and decreasing smoothly to *ca* 1–2 kcal/mole at the nematic to smectic A phase transition. This behavior is in accordance with the model discussed earlier which assumes pronounced pretransitional S_A character in the nematic phase and methane expulsion into the more fluid aliphatic regions of the S_A phase. The relatively large T_1 values and low apparent activation energy in the S_A phase are in accordance with the proton lineshapes in Figure 12, which indicate a relatively fluidic environment. The abrupt decrease in the aliphatic tail flexibility in the S_B phase is reflected in the decreasing T_1 values and increased activation energy in this phase from the results in Figure 14. As pointed

out in the Introduction, it is beyond the scope of this work to provide a quantitative analysis of the T_1 data. These measurements do, however, complement the qualitative picture drawn from the diffusion coefficients and signal splittings of the molecular dynamics of methane in liquid crystalline phases.

F. Diffusion of $CHCl_3$ in Phase 5 and 40.8

The results for chloroform diffusion in Phase 5, shown in Figure 15, are consistent with the trends observed for small solute diffusion in liquid crystals forming solely nematic phases. The activation energies were calculated to be $E_{\parallel} = 6.1 \pm 0.3$ kcal/mole and $E_{\perp} = 6.60 \pm 0.3$ kcal/mole (Table II), with diffusional anisotropies $D_{\parallel}/D_{\perp}$ varying from 1.2 at 48°C to 1.3 at 27°C. The activation energies for chloroform are greater than those for methane and DDE and lower than those observed for TTE and TMS in Phase 4/5.

The diffusion behavior of chloroform in 40.8, Figure 16, allows a qualitative comparison to the behavior found for methane in 40.6 (Figure 8). Most striking is the observation that $D_{\parallel} > D_{\perp}$ for chloroform in the nematic phase, in marked contrast to $D_{\parallel} < D_{\perp}$ in CH_4,

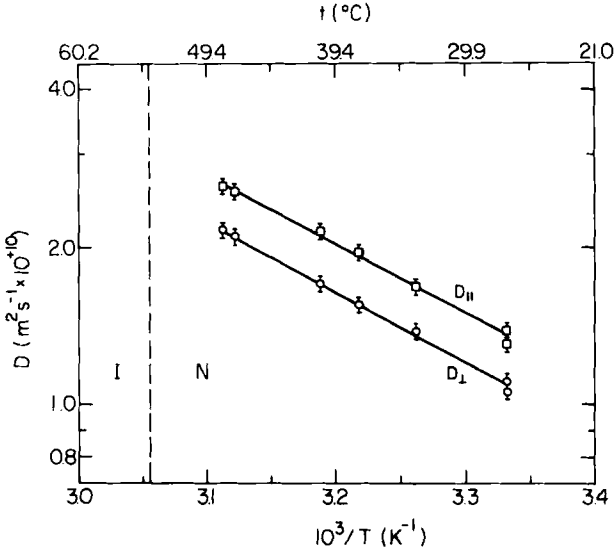

FIGURE 15 Arrhenius plots of chloroform diffusion coefficients in Phase 5, as explained in Figure 5.

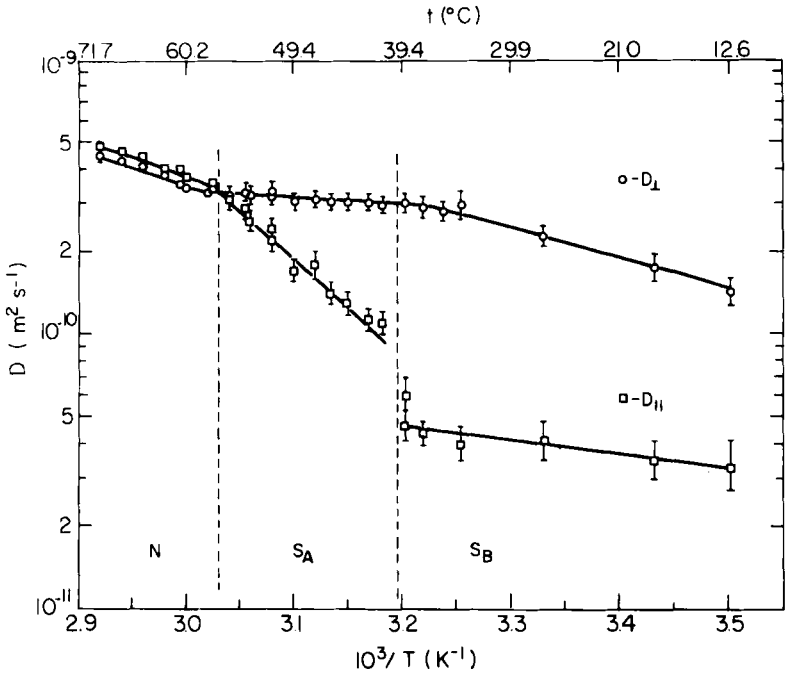

FIGURE 16 Arrhenius plots of chloroform diffusion coefficients in the nematic (N), smectic A (S_A) and smectic B (S_B) phases of 40.8.

which was reasoned to be due to strong pretransitional effects. It seems unlikely that this contrast is due to the difference in the 40.6–40.8 structures, since the added aliphatic chain length would tend to enhance the transverse diffusion by increasing the aliphatic volume fraction. Instead, the presence of a large solute which might interact strongly with the solvent could disrupt the local solvent structure; the observed phase transition temperatures in the $CHCl_3$-40.8 solution are depressed an average of 8°C relative to those of solvent. This depression reflects some disruption of the pronounced local smectic packing that was assumed to be influential in methane diffusion in the nematic phase of 40.6. Some residual precritical influence in the nematic phase of 40.8 may exist, however. The trend $E_\perp > E_{||}$ found for the strictly nematic systems is not observed in Figure 16, but instead $E_{||} = 7.7 \pm 0.8$ kcal/mole and $E_\perp = 6.3 \pm 0.7$ kcal/mole (Table II). This is to be expected in the presence of local smectic ordering, which would cause an increase $E_{||}$ and a decrease in $E_\perp$.

In the S_A phase of 40.8, the small apparent activation energy, $E_\perp = 1.3 \pm 0.5$ kcal/mole is probably the result of partial chloroform expulsion but the effect is not as obvious as for methane in 40.6 (Figure 8).

Local disordering may also explain the relatively low value of $E_\parallel = 16 \pm 2$ kcal/mole in the S_A phase of the 40.8 solution, compared to $E_\parallel = 33$ kcal/mole for methane diffusion in 40.6 (Table II). In the S_B phase of 40.8, activation energies for chloroform diffusion are listed in Table II and are again somewhat smaller than the corresponding values found for the CH_4-40.6 system.

G. Conclusions

Diffusion of methane or chloroform, dissolved in nematic, smectic A or smectic B phases of liquid crystals is anisotropic. This behavior reflects the anisotropic intermolecular potential prevailing in these systems. In detail, however, the behavior may vary from one system or phase to another. Our results point out to the following factors which seem to govern the magnitude and sign of the diffusional anisotropy:

a. For thermotropic materials which consist of a rigid aromatic core and more flexible aliphatic tails, methane and chloroform have different solubilities and different diffusion properties in these two regions of the solvent. The volume ratio of the aromatic to aliphatic regions in these solvents is therefore important in determining the overall diffusion behavior.

b. Order patterns in different liquid crystalline phases strongly affect the diffusion. Pretransitional effects, which sometimes range throughout the nematic phase, change these patterns locally and are clearly manifested in the results.

c. Solvent ordering may sometimes disturb the isotropic equilibrium solubility ratio between the aliphatic and aromatic regions and result in an "expulsion effect" which promotes solute migration to the aliphatic regions. Consequently the diffusional characteristics of aliphatic regions become more pronounced.

d. Solute volume and tendency to associate specifically with specific parts of the solvent (e.g. chloroform to benzene rings) have a marked influence on the diffusion behavior.

Qualitative formulation of these conclusions requires an extensive study of a large number of carefully selected solvent-solute systems.

Acknowledgments

The authors wish to thank Prof. Z. Luz and Dr. R. Poupko for the many helpful discussions during the course of this work. A. L. wishes to acknowledge the support of the Fund for the Promotion of Research at the Technion.

References

1. J. A. Murphy and J. W. Doane, *Mol. Cryst. Liq. Cryst.*, **13,** 93 (1971).
2. G. J. Krüger and H. Spiesecke, *Ber. Bunsenges. Physik. Chem.*, **75,** 272 (1971).
3. J. A. Murphy, J. W. Doane, Y. Y. Hsu and D. L. Fishel, *Mol. Cryst. Liq. Cryst.*, **22,** 133 (1973).
4. G. J. Krüger and H. Spiesecke, *Z. Naturforsch.*, **28a,** 964 (1973).
5. G. J. Krüger, H. Spiesecke and R. Van Steenwinkel, *J. Physique Colloq.*, **36,** C1-91 (1975).
6. G. J. Krüger and H. Spiesecke, *Ann. Phys.*, **3,** 193 (1978).
7. A. Loewenstein, *Chem. Phys. Lett.*, **38,** 543 (1976).
8. R. R. Vold, R. L. Vold and N. M. Szeverenyi, *J. Phys. Chem.*, **85,** 1934 (1981).
9. H. Y. Carr and E. M. Purcell, *Phys. Rev.*, **94,** 630 (1954).
10. E. O. Stejskal and J. E. Tanner, *J. Chem. Phys.*, **42,** 288 (1965).
11. D. S. Webster and K. H. Marsden, *Rev. Sci. Instrum.*, **45,** 1232 (1974).
12. W. Hayduk and W. D. Buckley, *Chem. Eng. Sci.*, **27,** 1997 (1972).
13. D. F. Evans, T. Tominaga and C. Chan, *J. Sol. Chem.*, **8,** 461 (1979).
14. C. S. Yannoni, *J.Chem. Phys.*, **51,** 1682 (1969).
15. R. Ader and A. Loewenstein, *Mol. Phys.*, **24,** 455 (1972).
16. D. Bailey, A. D. Buckingham, F. F. Fujiwara and L. W. Reeves, *J. Magn. Reson.*, **18,** 344 (1975).
17. A. Abragam, The Principles of Nuclear Magnetism, Clarendon Press, Oxford (1961).
18. G. W. Smith, Z. G. Gardlung and R. J. Curtis, *Mol. Cryst. Liq. Cryst.*, **19,** 327 (1973).
19. P. Keller and L. Liebert, "Liquid Crystal Synthesis for Physicists", in L. Liebert, Ed., *Liquid Crystals, Solid State Physics*, Suppl. 14, Academic Press, New York (1978).
20. H. Breuer, *Rev. Sci. Instrum.*, **36,** 1666 (1965).
21. G. Ödberg and L. Ödberg, *J. Magn. Reson.*, **16,** 342 (1974).
22. I. Zupancic and J. Pirs, *J. Phys. E: Sci. Instrum.*, **9,** 79 (1976).
23. M. I. Hrovat and C. G. Wade, *J. Magn. Reson.*, **45,** 67 (1981).
24. M. I. Hrovat and C. G. Wade, *J. Chem. Phys.*, **73,** 2509 (1980).
25. R. Mills, *J. Phys. Chem.*, **69,** 316 (1965).
26. I. Zupancic, J. Pirs, M. Luzar, R. Blinc and J. W. Doane, *Solid State Commun.*, **15,** 227 (1974).
27. E. Merck and W. Darmstadt, Germany, Data sheets on Nematic Phase 4 and Nematic Phase 5 (1977).
28. H. Ertl, R. K. Ghai and F. A. L. Dullien, *AIChE J.*, **19,** 881 (1973).
29. H. Ertl, R. K. Ghai and F. A. L. Dullien, *AIChE J.*, **20,** 1 (1974).
30. H. Kreppe and F. Schneider, *Mol. Cryst. Liq. Cryst.*, **65,** 23 (1980).
31. H. Kneppe, F. Schneider and N. K. Sharma, *Ber. Bunsenges. Phys. Chem.*, **85,** 784 (1981).
32. W. H. de Jeu, *Physical Properties of Liquid Crystalline Materials*, Gordon and Breach, New York (1980).

33. A. J. Leadbetter, R. M. Richardson and C. N. Colling, *J. Physique Colloq.*, **36,** C1-37 (1975).
34. A. J. Leadbetter, J. C. Frost, J. P. Gaughan, G. W. Gray and A. Mosley, *J. Physique*, **40,** 375 (1979).
35. B. Deloche and J. Charvolin, *J. Physique*, **37,** 1497 (1976).
36. K. Chu, N. K. Ailawadi and D. S. Moroi, *Mol. Cryst. Liq. Cryst.*, **38,** 45 (1977).
37. D. E. Moncton and R. Pindak, *Phys. Rev. Lett.*, **43,** 701 (1979).
38. J. D. Litster, in *Liquid Crystals of One- and Two-Dimensional Order*, eds. W. Helfrich and G. Heppke, Springer-Verlag, Berlin (1980), pp. 65–70.
39. W. Lin and J. H. Freed, *J. Phys. Chem.*, **83,** 379 (1979).
40. E. E. Burnell and C. A. de Lange, *J. Magn. Reson.*, **39,** 461 (1980); E. E. Burnell and C. A. de Lange, *Chem. Phys. Lett.*, **76,** 268 (1980); E. E. Burnell and C. A. de Lange, Proc. Ismar-Ampere Conference, *Bull. Magn. Reson.*, **2,** 2289 (1980); J. W. Emsley and G. R. Luckhurst, *Mol. Phys.*, **41,** 19 (1980).